

Experimental Investigations on Slurry Erosion Behaviour of HVOF and HVOLF Sprayed Coatings on Hydraulic Turbine Steel

Harjinder Singh¹ · Khushdeep Goyal¹ · Deepak Kumar Goyal²

Received: 15 August 2015 / Accepted: 30 August 2016 / Published online: 9 September 2016
© The Indian Institute of Metals - IIM 2016

Abstract Slurry erosion behaviour of high velocity oxy fuel (HVOF) and high velocity oxy liquid fuel (HVOLF) sprayed coatings on hydraulic turbine material (i.e. CA6NM steel) was investigated at different levels of various parameters. The 50 % (WC–Co–Cr) and 50 % (Ni–Cr–B–Si) coating powder was deposited on CA6NM steel samples by HVOF and HVOLF thermal spraying techniques. Erosion tests were conducted on self-made erosion test rig with various factors as explained in the “experimentation” section. Coated and uncoated samples of CA6NM steel were investigated by following a design of experiments based on the L_9 Taguchi technique, which was used to obtain the data of erosion test in a controlled way. Four parameters used in L_9 experiment were velocity, impact angle, slurry concentration and average particle size. The study revealed that the velocity, impact angle and slurry concentration were most significant among various parameters, influencing the wear rate of the coatings. The average particle size did not show any significant effect on both the coatings. In comparison, coated samples showed approximately two times better results in erosion resistance than uncoated samples. Scanning electron microscopy of eroded surface showed different mechanisms of erosion on different samples under various conditions.

Keywords Erosion · Turbine steel · Coatings · Slurry · Impact

✉ Khushdeep Goyal
khushgoyal@yahoo.com

¹ Department of Mechanical Engineering, Punjabi University, Patiala 147002, India

² Department of Mechanical Engineering, IK Gujral Punjab Technical University, Kapurthala, Punjab, India

1 Introduction

Slurry erosion is defined as the degradation of surface by impingement of solid particles suspended in a liquid medium [1]. Slurry erosion is affected by various parameters such as velocity of flow, impingement angles, shape and size of particles, mechanical properties of surface as well as particles, and defects in the surface [2]. It is the major cause for failure of hydraulic components of fluid machineries [3]. The Indian hydro power stations located in Himalayan region results in economical loss in the order of US\$ 120–150 million a year due to repair, reduced efficiency, and forced outages [2, 4–6]. In the peak of monsoon seasons, these plants have to be shut down for maintenance and repairs. The most affected parts of hydroturbines are impellers, guide vanes, buckets, nozzles, spears and labyrinth seal [2, 4].

CA6NM (13/4) (ASTM 743) is commonly used material in hydroturbines due to its good corrosion and cavitation erosion resistance and high impact and fracture toughness [7–9]. A number of research papers are available on slurry erosion, but research related to 13/4 steel is limited [2]. Harsha et al. [10] studied the erosion behaviour of ferrous and nonferrous materials and also examined the erosion model developed for normal and oblique impact angles by Hutchings. Erosion studies of ferrous and non-ferrous materials were conducted at different impingement angles (15°–90°) and impact velocities (24–52 m/s). It was observed that the erosion peak at about 60° impingement angle occurred at higher impact velocity (52 m/s) for different materials. Hidalgo et al. [11] carried out the behaviour of plasma sprayed NiCrBSiFe and WC–NiCrBSiFe alloys biased to conditions which acted as a post-combustion gas atmosphere from a coal-fired boiler combustor. The study evaluated the effects of thermal exposure at high

temperatures on the microstructure of the coatings and on the adherence between substrate (austenitic stainless steel) and coatings and also examined the oxidation rates of these coatings in atmospheres with 3–3.5 % of free oxygen at 773 and 1073 K. Tabbara et al. [12] attracted the attention towards high velocity oxy liquid fuel (HVOLF) due to their advantage of producing denser coatings in comparison to their gas-fuelled counterparts. Singh et al. [5] investigated the erosive wear behaviour of hydraulic turbine material i.e. CA6NM samples coated by (50 %) WC–Co–Cr and (50 %) Ni–Cr–B–Si powder with plasma thermal spray technique. They concluded that the impact velocity, slurry concentration and impact angle were most significant factors influencing the wear rate of these coatings. Chauhan et al. [13] investigated the use of martensitic stainless steel (termed as 13/4) in the fabrication of underwater parts in hydroelectric projects. However, there were several maintenance problems associated with the use of this steel. A nitronic steel (termed as 21–4–N) was developed as an alternative with the specific aim of overcoming these problems. A comparative study was conducted on the erosion behavior of 13/4 and 21–4–N steels by means of solid particle impingement using gas jet.

Goyal et al. [14] evaluated the effect of two HVOF sprayed coatings on slurry erosion behavior of CF8M steel. Two coatings of WC–10Co–4Cr and $\text{Al}_2\text{O}_3 + 13\text{TiO}$ were deposited with HVOF spray process on the base material CF8M turbine steel. The effect of three parameters: particle size, speed and slurry concentration on slurry erosion of this material was investigated. The bare steel and $\text{Al}_2\text{O}_3 + 13\text{TiO}$ coating followed ductile and brittle mechanisms whereas the WC–10Co–4Cr coating showed the mixed behavior (mainly ductile). $\text{Al}_2\text{O}_3 + 13\text{TiO}_3$ coating was found to be useful to increase the slurry erosion resistance of steel. Ji et al. [15] deposited Cr_3C_2 –NiCr coatings by HVOF process with different spray parameters and investigated the micro-structural factors, as characterized by scanning electron microscopy (SEM) and transmission electron microscopy (TEM), in relation to the abrasive wear of the coatings. Solnordal et al. [16] used silica flour suspended in air and impacting samples of stainless steel of grade 316 and 304, at nominal flow velocities of 60 and 80 m/s. Analysis indicated that the impact velocity magnitude and angle were affected by local carrier gas velocity for particles below 32.5 μm in size, even though Stokes number was greater than ten. In the case examined, over 82 % of erosion was caused by particles larger than 32.5 μm . Cantera et al. [17] compared the fracture toughness of two thermally sprayed tungsten carbide-cobalt-chromium coatings of nominally identical composition (86WC–10Co–4Cr), one produced by the Detonation Gun (D-Gun) process and other by the HVOF process, by the indentation method. Grewal et al. [18]

deposited HVOF deposited Al_2O_3 in Ni coatings. The authors concluded that the erosion resistance of 40 wt% Alumina was highest. The coating was able to increase the erosion resistance by 2–4 times that of uncoated specimen.

It has been observed from the literature review that no systematic indepth studies have been found on 13/4 steels. It is important to investigate how 13/4 steel behaves under different experimental conditions. These investigations can help to improve the performance of this steel.

2 Experimental Details

2.1 Material

The steel mostly used in modern turbine industry i.e. 13Cr4Ni or CA6NM grade of ASTM 743 steel was used for testing purpose. This steel was procured from Mithila Mal-leables Pvt. Ltd., Sirhind (Punjab, India). The dimension of the samples was kept as 50 mm \times 30 mm \times 10 mm. The surface of each sample was finished by surface grinder. Table 1 shows the chemical composition of CA6NM steel.

CA6NM steel is also known as martensitic steel. The nominal values of some of its mechanical properties as hardness, tensile strength and yield strength are given in the Table 2.

2.2 Deposition of Coating

The HVOF and HVOLF thermal spray techniques were used for coating. One side of the sample was used for testing of coated and uncoated materials. The coating of 50 % (WC–Co–Cr) and 50 % (Ni–Cr–B–Si) powder over the samples was done with HVOF (Hipojet) and HVOLF (MJP 5000) techniques, from Metalizing Equipments Company Pvt. Ltd., Jodhpur. The SEM analysis of powder is shown in Fig. 1. Before applying the coatings, the samples were grit blasted with alumina grit (Al_2O_3) of 16 mesh size at pressure of 5 kg/cm² using abrasive blasting machine. Blasting of samples is necessary before applying the coating so as to supplement the adhesion of the coatings to the surface of sample. The thickness of coating was 250 μm which was measured by micrometer.

2.3 Test Apparatus

The test rig as shown in Fig. 2 consisted of a centrifugal pump, conical tank, nozzle, specimen holder, valves and pressure gauge. Centrifugal pump driven by 5 HP, 1500 rpm electric motor had a capacity of max pressure 13.5 bar at a discharge of 240 l/min. Slurry was re-circulated during the test. During the test, the temperature of slurry increased to a certain level and thereafter remained

Table 1 Composition of CA6NM steel

Element	C	Si	Mn	P	S	Cr	Mo	Ni	Co	V	Fe
Percentage (%)	0.030	0.639	0.166	0.021	0.004	12.92	0.594	3.05	0.055	0.006	82.41

Table 2 Nominal values of mechanical properties of CA6NM

Material	Brinell hardness (in HBW)	Tensile strength (in MPa)	Yield strength (in MPa)
CA6NM	269	755	550

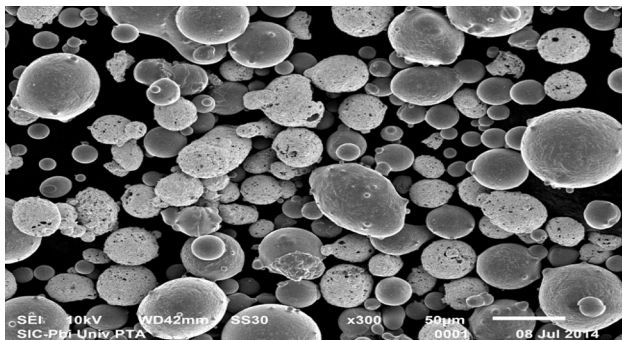


Fig. 1 SEM analysis of 50 % (WC–Co–Cr) and 50 % (Ni–Cr–B–Si) coating powder

constant, which was due to mechanical action of pump. The temperature was controlled by using ice around the slurry tank. The flow rate of the slurry was controlled with the help of main valve and bypass regulator valve between the delivery side and nozzle. The rectangular tapered tank having 600 × 450 mm at top which converged to 100 × 100 mm at the bottom through a length of 1200 mm was used to store the slurry. A mesh was provided in the bottom of the tank to avoid the object from falling into the tank and get struck inside the pipeline.

2.4 Experimental Design

Table 3 shows the design of L₉ orthogonal array and Table 4 shows various levels of different parameters.

3 Results and Discussion

3.1 Comparison of Erosion Performance at Various Runs for HVOF and HVOLF Coated and Uncoated Samples of CA6NM Steel

The plots as shown in Figs. 3, 4 and 5 clearly indicate that erosion rate for run 1 is least and erosion rate for run 3 is most among the all nine runs for HVOF coated, HVOLF coated and uncoated samples. The Fig. 3 for HVOF shows

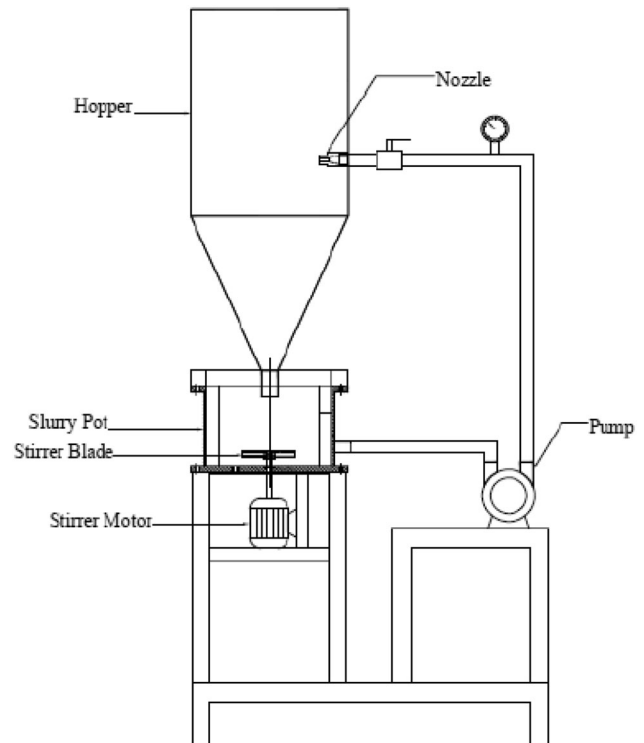


Fig. 2 Jet erosion tester Schematic diagram [19]

that there is no significant effect of erosion rate for initial 60 min, but later it changes significantly for various runs. The plot also depicts that there is a little difference in erosion rate for run 2, run 4, run 6, run 7 and run 8 as different levels of parameters plays a decisive role. The Fig. 4 for HVOLF shows that a significant change in erosion seems to occur after initial 90 min as the plot shows a shape of contracting V up to this time. This plot also shows similar results as for HVOF with a little change. Whereas, Fig. 5 indicates that the erosion is higher for uncoated samples than the coated samples. The erosion rate graph shows a shape of V for uncoated samples at various runs for the entire period of 180 min except run 3 and run 9. These findings are similar to those reported by many researchers [2, 4, 13, 20].

Table 3 L₉ orthogonal array of Taguchi method for experimentation design

Various runs	Particle size	Concentration	Velocity	Impact angle
Run 1	A1	B1	C1	D1
Run 2	A1	B2	C2	D2
Run 3	A1	B3	C3	D3
Run 4	A2	B1	C2	D3
Run 5	A2	B2	C3	D1
Run 6	A2	B3	C1	D2
Run 7	A3	B1	C3	D2
Run 8	A3	B2	C1	D3
Run 9	A3	B3	C2	D1

Table 4 Different values of parameters

Particle size (in μm)	Concentration (in ppm)	Velocity (in m/s)	Impact angle (in °)				
A1	150	B1	10,000	C1	20	D1	30
A2	250	B2	20,000	C2	40	D2	60
A3	350	B3	30,000	C3	60	D3	90

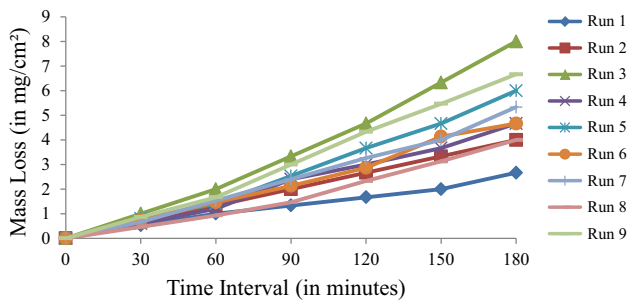


Fig. 3 Comparison of various runs for HVOF coated samples

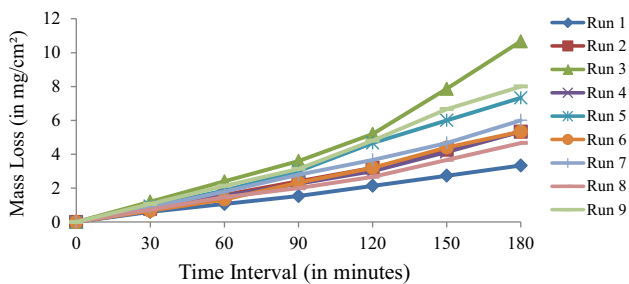


Fig. 4 Comparison of various runs for HVOLF coated samples

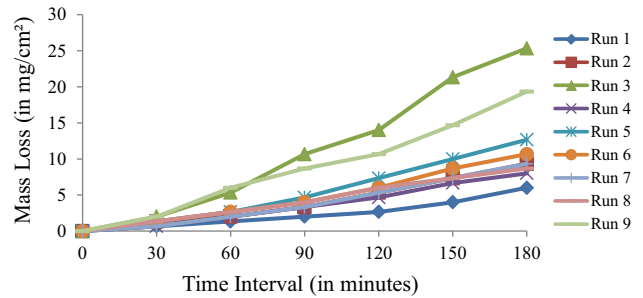


Fig. 5 Comparison of various runs for uncoated CA6NM steel samples

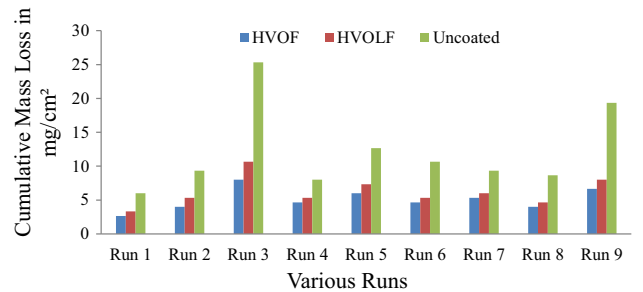


Fig. 6 Comparison of cumulative erosion performance of different samples at various runs

3.2 Comparison of Cumulative Erosion Performance of HVOF and HVOLF Coated and Uncoated Samples of CA6NM steel at Various Runs

Figure 6 indicates a comparison of cumulative mass loss (in mg/cm²) for various runs of HVOF and HVOLF coated and uncoated samples. This chart illustrates that maximum erosion is for the uncoated samples and HVOF coated samples show slightly better results than the HVOLF coated samples. The erosion rate of run 3 is most among the all nine runs. Run 9 results the second highest erosion rate. The erosion rate for all the coated samples lies below 10 mg/cm². The performance of coated sample is approximately two times better than uncoated samples. These findings are similar to that reported by many researchers [2, 4, 21].

3.3 Effect of Various Parameters on Slurry Erosion for Different Samples of CA6NM Steel

3.3.1 Effect of Velocity on Slurry Erosion

To evaluate the effect of velocity on slurry erosion, tests have been conducted at three different levels of velocity

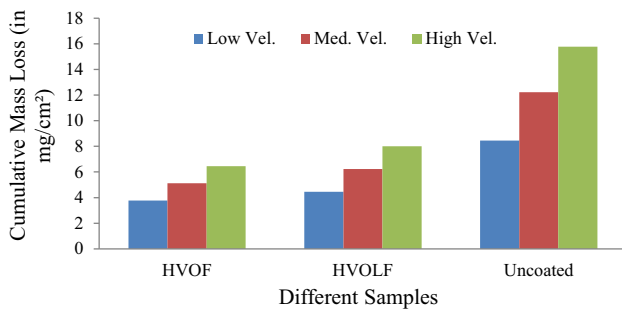


Fig. 7 Effect of velocity on slurry erosion for different samples

(20, 40 and 60 m/s). The effect of velocity can be calculated by measuring the cumulative mass loss at each level of velocity. The effect of velocity on slurry erosion is shown in Fig. 7.

As the erosion wear occurs due to the movement/kinetic energy of impacting particles, so it is quite expected that the erosion rate will increase with the increase in the velocity of impacting particles. This fact has already been proved by researchers [2, 5, 14, 20] on the basis of their experimental studies. This plot indicates that with the increase in velocity, the erosion rate of HVOF and HVOLF coated and CA6NM steel increases. The reason behind this may be that when impacts take place at low impact velocity, the rebounding particles are able to de-accelerate and divert the incoming particles more effectively. However, when the velocity of impact is high, the rebounding particles are not able to interact with the incoming particles with similar intensity, as is the case during low-velocity impacts. These findings are similar to as reported by many researchers [2, 4, 5, 14, 20, 22].

3.3.2 Effect of Impact Angle on Slurry Erosion

To evaluate the effect of impact angle on slurry erosion, tests have been conducted at three different levels of angle (30°, 60° and 90°). The effect of angle can be calculated by measuring the cumulative mass loss at each level of angle. The effect of impact angle on slurry erosion is shown in Fig. 8.

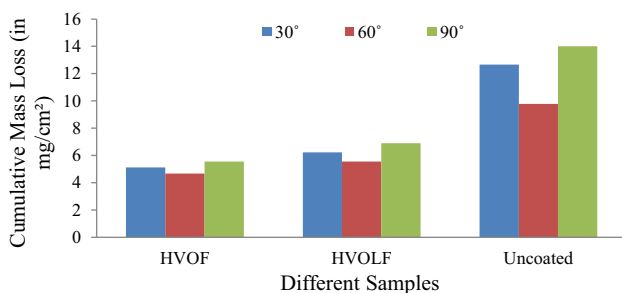


Fig. 8 Effect of impact angle on slurry erosion for different samples

The mechanism behind material removal by slurry erosion depends upon the material properties and the angle at which the erodent strikes the target surface. Goyal et al. [14] suggested that material removal from the surface of ductile materials occurs by a process of direct micro-cutting or plastic deformation, followed by cutting. This plot indicates that the maximum erosion rate is at 90° and minimum at 60° angle. This graph also illustrates that erosion rate at 30° is slightly lower than 90°. The reason behind this may be as suggested by Grewal et al. [2] that at 90° impingement angle, platelet mechanism and formation of deep craters play an important role in erosion mechanism, whereas at 30° angle, ploughing along with proposed mixed cutting and ploughing mechanism may be responsible for the removal of the material. While for 60°, ploughing may be responsible as the impact energy of the particles make the material deform plastically. This plastically deformed material particles, spherical in shape, affect the material displacement and get accumulated towards the end from where the particle leaves. These findings are similar to as reported by many researchers [2, 14, 20].

3.3.3 Effect of Level of Slurry Concentration on Slurry Erosion

To evaluate the effect of level of slurry concentration on slurry erosion, tests have been conducted at three different levels of concentration (10,000, 20,000 and 30,000 ppm). The effect of concentration can be calculated by measuring the cumulative mass loss at each level of concentration. The effect of slurry concentration on slurry erosion is shown in Fig. 9.

As the liquid droplets contain solid particles, the presence of suspended sand particles makes the erosive attack more severe. Increasing the sand content simply increases the severity of erosive/abrasive attack as a greater number of sand particles are impinging on the surface. The problem is so severe that some of these plants need to be shut down to avoid significant damage

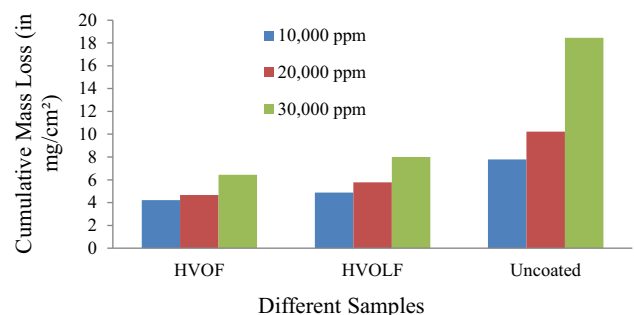


Fig. 9 Effect of level of slurry concentration on slurry erosion for different samples

to the submerged parts during monsoon season due to a considerable increase in the concentration of sand. It is clear from the plot that when the sand concentration is 10,000 ppm, the erosion rate is least among all the coated as well as uncoated samples. On increasing the slurry concentration to 20,000 ppm, the slurry erosion rate further increases. When the sand concentration further increases to 30,000 ppm, there is a greater increase in the slurry erosion rate. While, the coated samples show a much improved performance than the uncoated sample. These findings are similar to as reported by many researchers [2, 4, 5, 14, 20].

3.3.4 Effect of Average Particle Size on Slurry Erosion

To evaluate the effect of average particle size on slurry erosion, tests have been conducted at three different levels of particle size (150, 250 and 350 μm). The effect of particle size can be calculated by measuring the cumulative mass loss at each level of average particle size. The effect of average particle size on slurry erosion is shown in Fig. 10.

This plot indicates that particle size has no significant effect on mass loss due to slurry erosion. The reason for this is because, as the particle increases in size, the surface area of the particle increases as well. This means that there is more particle surface area which will come in contact with the metal surface upon impact. This in turn, will lead to the ‘force upon impact’ being spread over a wider area. Also the larger particles at the metal surface may hinder other particles from coming in contact with the surface. This will lead to a shallower depth of penetration and therefore the erosion damage will not significantly change even though the mass and size of the particle is greater. While, it is clear from the plot for uncoated sample that fine particles are able to erode most as the number of particles increases during impact. These findings are similar to as reported by many researchers [5–7, 17, 23].

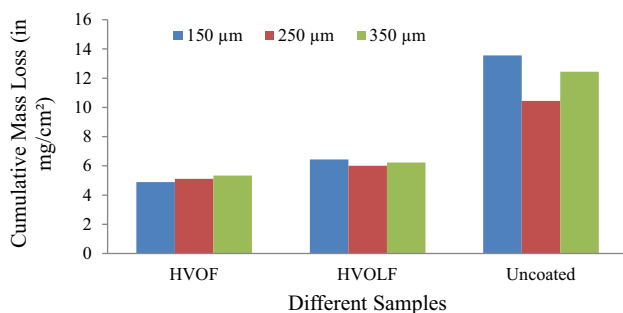


Fig. 10 Effect of average particle size on slurry erosion for different samples

3.4 SEM Analysis

3.4.1 SEM Analysis of Unperformed Samples for HVOF and HVOLF Sprayed 50 % (WC–Co–Cr) and 50 % (Ni–Cr–B–Si) Coating Deposited and Uncoated Samples of CA6NM Steel

The SEM analysis are shown in Figs. 11, 12 and 13 for HVOF and HVOLF sprayed 50 % (WC–Co–Cr) and 50 % (Ni–Cr–B–Si) coating deposited on CA6NM steel sample and uncoated CA6NM steel respectively. The coated

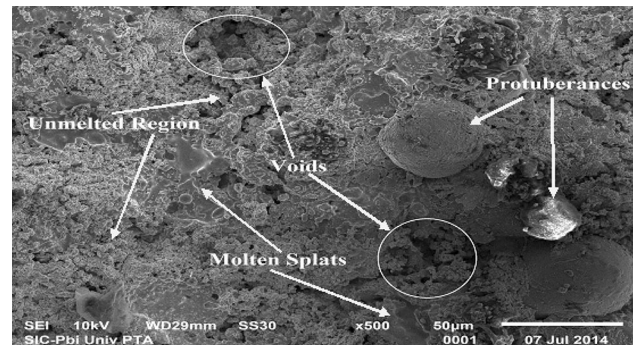


Fig. 11 SEM analysis of HVOF sprayed 50 % (WC–Co–Cr) and 50 % (Ni–Cr–B–Si) coating deposited on CA6NM steel

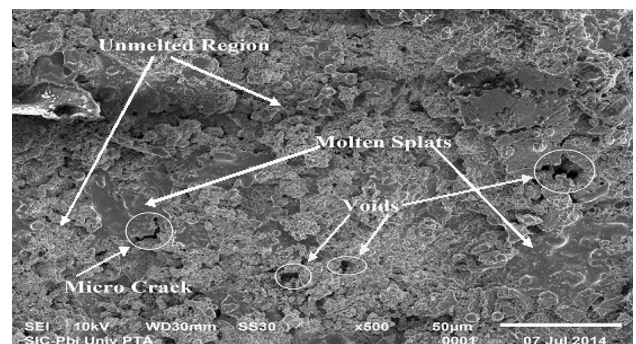


Fig. 12 SEM analysis of HVOLF sprayed 50 % (WC–Co–Cr) and 50 % (Ni–Cr–B–Si) coating deposited on CA6NM steel

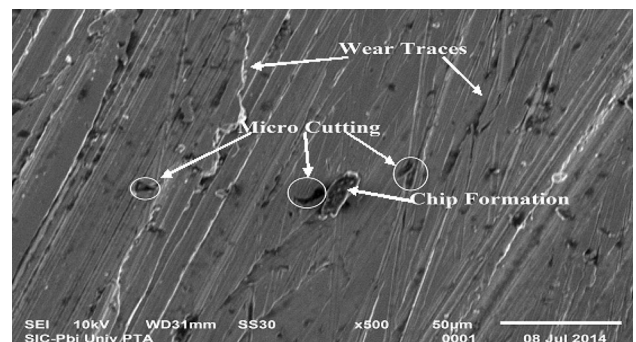


Fig. 13 SEM analysis of uncoated sample of CA6NM steel

samples clearly indicate that the coating is found to have a laminar splat-like cross-sectional microstructure, which is a typical feature of thermal spray coatings. The coating in general has a nearly uniform surface micro-structure, consisting of interlocked splats. Some very fine un-melted particles seem to be embedded in molten splats at some locations. The surface micrograph of coating samples seem to have micro voids present in them. The Fig. 11 for HVOF indicates protuberances at some locations. While, Fig. 13 for uncoated sample shows some marks of wear traces and micro cuttings, may be produced during surface finishing of the sample.

3.4.2 SEM Analysis of HVOF Coated Samples Performed at Various Conditions

The SEM analysis for HVOF coated sample at maximum velocity, 250 μm particle size and 20,000 ppm concentration impacting at 30° is shown in Fig. 14. It indicates that the erosion is mainly due to platelets, wherein mixed cutting and ploughing mode come into action. Figure 15 shows SEM analysis at maximum velocity, 10,000 ppm

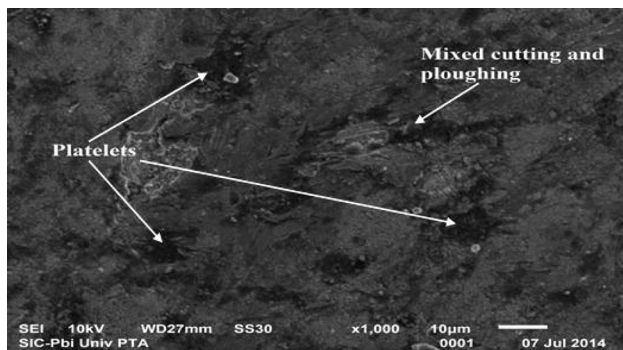


Fig. 14 SEM analysis of HVOF sprayed 50 % (WC–Co–Cr) and 50 % (Ni–Cr–B–Si) coating deposited on CA6NM steel at 30° impact angle for maximum velocity, 20,000 ppm and 250 μm of particle size

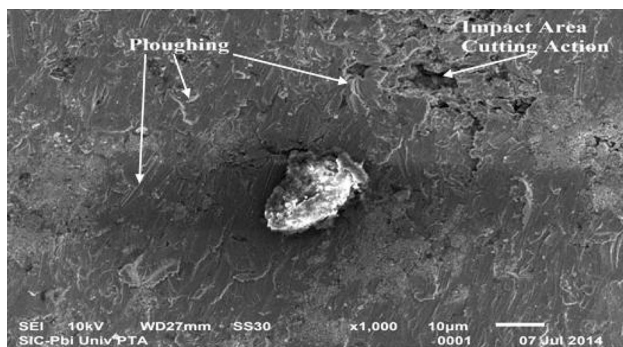


Fig. 15 SEM analysis of HVOF sprayed 50 % (WC–Co–Cr) and 50 % (Ni–Cr–B–Si) coating deposited on CA6NM steel at 60° impact angle, 60 m/s of velocity, 10,000 ppm concentration and 350 μm of particle size

concentration and 350 μm particle size. It shows that the erosion takes place due to cutting action and ploughing may be due to the fact that heavy particles at maximum velocity results into the cutting action. Figure 16 shows that the erosion is mainly due to craters, platelets and deep crater and some of wear traces.

3.4.3 SEM Analysis of HVOF Coated Samples Performed at Various Conditions

The SEM analysis as shown in Fig. 17 indicates that the erosion mechanism is mainly due to ploughing, lip formation and platelets. Figure 18 indicates that the erosion is mainly due to cutting action which may result from the continuous impingement of fine particles with 20,000 ppm concentration impacting at 60° with a speed of 40 m/s at the same point. While the Fig. 19 for 90° indicates that the erosion is mainly due to deep crater, Platelets of small size and micro cutting at some locations.

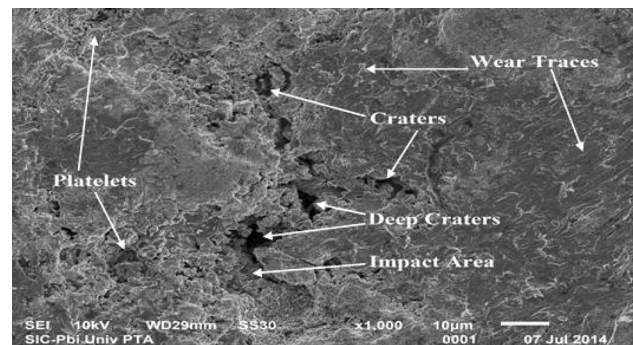


Fig. 16 SEM analysis of HVOF sprayed 50 % (WC–Co–Cr) and 50 % (Ni–Cr–B–Si) coating deposited on CA6NM steel at 90° impact angle, 60 m/s of velocity, 30,000 ppm concentration and 150 μm of particle size

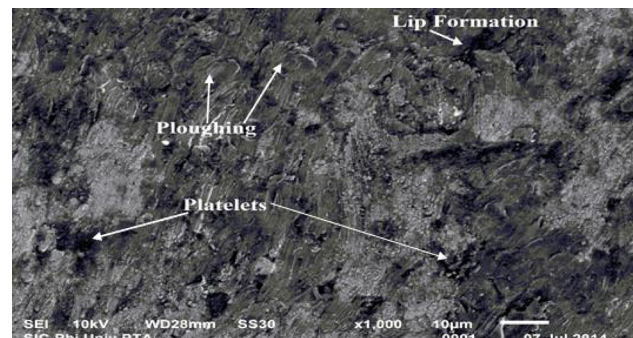


Fig. 17 SEM analysis of HVOF sprayed 50 % (WC–Co–Cr) and 50 % (Ni–Cr–B–Si) coating deposited on CA6NM steel at 30° impact angle for 20 m/s of velocity, 10,000 ppm of concentration and 150 μm of particle size

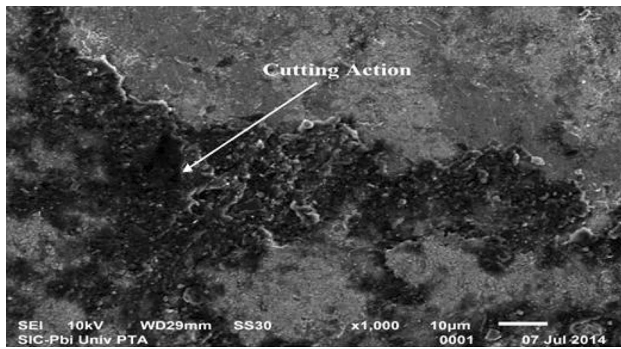


Fig. 18 SEM analysis of HVOLF sprayed 50 % (WC–Co–Cr) and 50 % (Ni–Cr–B–Si) coating deposited on CA6NM steel at 60° impact angle for 40 m/sec of velocity, 20,000 ppm of concentration and 150 µm of particle size

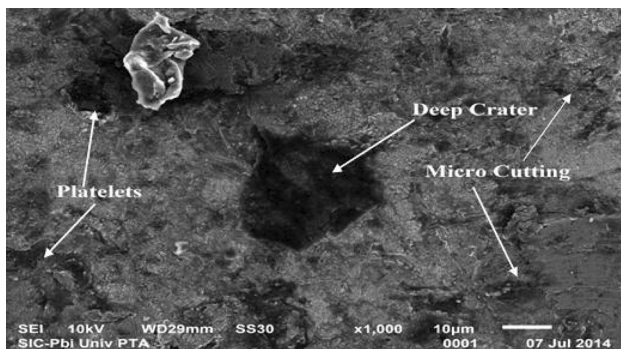


Fig. 19 SEM analysis of HVOLF sprayed 50 % (WC–Co–Cr) and 50 % (Ni–Cr–B–Si) coating deposited on CA6NM steel at 90° impact angle for 40 m/s of velocity, 10,000 ppm concentration and 250 µm of particle size

4 Conclusions

The effect of various parameters on slurry erosion mechanism of uncoated, HVOF and HVOLF coated CA6NM steel was investigated. The important conclusions drawn from the investigation are:

- The comparisons of mass loss show that erosion rate of CA6NM steel is more than HVOF and HVOLF coated samples.
- HVOF and HVOLF techniques give us the possibility of depositing 50 % (WC–Co–Cr) and 50 % (Ni–Cr–B–Si) coating powder on CA6NM steel.
- Erosion wear rate reduces with coatings.
- For all coated and uncoated steel samples, the maximum erosion is at 90° impact angle and minimum at 60°.
- The erosion mechanism of CA6NM steel under normal impact is due to craters and platelet mechanism but for 30° impact angle the platelets, micro cutting and ploughing comes into action.

- With increase in level of concentration of the particles, the mass loss increases for all the coated and uncoated steel samples.
- The average particle size do not have a significant effect on the coated samples but for uncoated samples, erosion rate is higher for fine particles than the coarse particles. This may be due to the fact that the large size hinders the fine particles to impact.
- For all the coated and uncoated samples, the erosion is mainly affected by velocity, slurry concentration, impact angle and particle size.
- For comparison between the coated and uncoated CA6NM steel, the following order of erosion rate has been observed.

CA6NM (HVOF) < CA6NM (HVOLF) < CA6NM uncoated steel

Acknowledgments This research received no specific grant from any funding agency in the public, commercial, or not-for-profit sectors.

References

1. Humphrey J, *Int J Heat Fluid Flow* **11** (1990) 170.
2. Grewal H, Agrawal A, and Singh H, *Tribol Lett* **52** (2013) 287.
3. Khurana S, Varun, and Kumar A, *Int J Ambient Energy* **50** (2015) 1.
4. Goyal D, Singh H, and Kumar H, *Proc Inst Mech Eng J J Eng Tribol* (2011) 1350650111412443.
5. Singh H, Goyal K, and Goyal D K, *Manuf Sci Technol* **2** (2014) 81.
6. Kumar L, Parashar C, and Kaur S, *Int J Eng Sci Res I* **4** (2013) 963.
7. Iwabuchi Y, and Sawada S, in *Stainless Steel Castings*, ed: ASTM International (1982).
8. Gysel W, Gerber E, and Trautwein A, in *Stainless Steel Castings*, ed: ASTM International (1982).
9. Goyal D K, Singh H, Kumar H, and Sahni V, *J Therm Spray Technol* **21** (2012) 838.
10. Harsha A, and Bhaskar D K, *Mater Des* **29** (2008) 1745.
11. Hidalgo V H, Varela F B, Menéndez A C, and Martinez S P, *Tribol Int* **34** (2001) 161.
12. Tabbara H, and Gu S, *Surface Coat Technol* **204** (2009) 676.
13. Chauhan A K, Goel D, and Prakash S, *Bull Mater Sci* **31** (2008) 115.
14. Goyal D K, Singh H, Kumar H, and Sahni V, *Wear* **289** (2012) 46.
15. Ji G-C, Li C-J, Wang Y-Y, and Li W-Y, *Surface Coat Technol* **200** (2006) 6749.
16. Solnordal C B, Wong C Y, Zamberi A, Jadid M, and Johar Z, *Wear* **305** (2013) 205.
17. Cantera E L, and Mellor B, *Mater Lett* **37** (1998) 201.
18. Grewal H, Agrawal A, Singh H, and Shollock B, *J Therm Spray Technol* **23** (2014) 401.
19. Thakur P A, Khairnar H S, Deore E, and More S, *Int J Novel Res Eng Sci* **2** (2014) 14–20.
20. Bhandari S, Singh H, Kumar H, and Rastogi V, *J Therm Spray Technol* **21** (2012) 1054.
21. Singh A, Viridi R L, and Goyal K, *Manuf Sci Technol* **2** (2014) 111.
22. Singh G, Viridi R L, and Goyal K, *Univ J Mech Eng* **3** (2015) 52.
23. Grewal H S, Bhandari S, and Singh H, *Metall Mater Trans A* **43** (2012) 3387.